IEEE Access
Multidisciplinary | Rapid Review | Open Access Journal

Received March 4, 2022, accepted March 15, 2022, date of publication March 21, 2022, date of current version March 24, 2022.

Digital Object Identifier 10.1109/ACCESS.2022.3160831

A Four-Port CSRR-Loaded Dual-Band MIMO Antenna With Suppressed Higher Order Modes

JOGESH CHANDRA DASH, (Member, IEEE), AND DEBDEEP SARKAR, (Member, IEEE)
Department of Electrical Communication Engineering, Indian Institute of Science, Bengaluru 560012, India

Corresponding author: Jogesh Chandra Dash (jcdash92@gmail.com)

This work was supported in part by the Infosys Young Investigator Grant, endowed by Infosys Foundation, Bengaluru, India.

ABSTRACT In this paper, we propose a compact four-port dual-band MIMO antenna with suppressed higher order modes (HOMs). First, complementary split ring resonator (CSRR) loading is used on a square microstrip antenna to achieve simultaneous miniaturization and dual-band response. Next, the HOMs in the proposed CSRR loaded MIMO configuration are analysed using equivalent circuit model as well as surface current distribution plots. By placing a single shorting post close to antenna center line, these HOMs of the four-port dual-band MIMO antenna are then suppressed, while maintaining satisfactory mutual coupling (<-11 dB) and impedance matching (<-15 dB) performance in the operating band. Furthermore, simulated and measured values of total active reflection coefficient (*TARC*), envelop correlation coefficient (*ECC*) and channel capacity loss (*CCL*) are within the desired levels of -10 dB, 0.5 and 0.5 bits/s/Hz respectively, signifying good diversity performance of the proposed MIMO antenna.

INDEX TERMS Complementary split ring resonator (CSRR), higher order modes (HOMs), microstrip antenna, multiple input multiple output (MIMO).

I. INTRODUCTION

Over the years, microstrip antennas have emerged as popular choice in wireless communication community because of its low profile, high gain, good front-to-back lobe ratio, low cost and ease of fabrication [1]. However, since microstrip antennas designed on PCBs (printed circuit boards) are essentially dielectric loaded cavities, higher order modes (HOMs) or harmonics get naturally excited in these structures [1]. This HOM excitation in microstrip antennas lead to electromagnetic interference and compatibility (EMI/EMC) issues in integrated circuits and systems where they are deployed [2]. Various techniques have been proposed to mitigate the problem of HOMs/harmonics excitation for single-element microstrip antennas [3]–[10]. In [3], a periodic 2D-photonic band gap (PBG) pattern is designed in the ground plane beneath a square microstrip antenna and harmonic suppression is demonstrated. In [4], a cavity-backed antenna is proposed with a filter directly inserted inside the antenna cavity at the feed position to suppress the HOMs. Similarly, a LC-trap filter is used in [5] to reduce the HOMs of the lower operating band in a single-fed planar inverted-F antenna. Different other techniques like use of shorting pin and slots [6], defected ground structure (DGS)-integrated feed [7], pair of quarter wavelength resonator with capacitive feeding structure [8], hairpin filter [9], integration technique with PIFA (planar inverted-F Antennas) [10] etc, have also been reported for HOM suppression in microstrip antennas. It is very well known that the non-linear active components such as power amplifier (PA) (in a Tx module) and low-noise-amplifier (LNA) and local oscillator (LO) (in a Rx module) are a few prime sources of spurious harmonic generation in a RF transceiver [11], [12]. Apart form these non-linear components, as mentioned earlier the passive component like microstrip antenna also equally responsible for harmonic generation in a transceiver module [1]–[10].

However, to the best of authors' knowledge, studies in open literature on the effect of antenna HOM and its reduction techniques mostly focus on single-band single-antenna systems. Since, the wireless communication systems in 5G networks and beyond rely on multi-antenna configurations (arrays, multiple-input multiple-output or MIMO) both for

The associate editor coordinating the review of this manuscript and approving it for publication was Qi Luo.

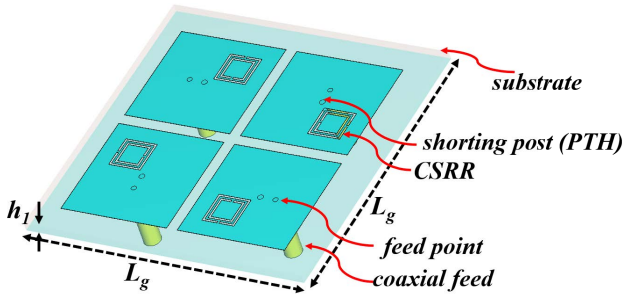

FIGURE 1. Schematic representation of HD and FD wireless communication systems.

transmitter and receiver modules, exploration of techniques to mitigate HOM effects in multi-band MIMO antennas becomes essential. The expected number of antennas for 5G user equipment (UE) is nearly 4-8 while the 5G base station focuses on larger scale antenna or massive-MIMO implementation, where the expected antenna number is nearly 100 or more [13]–[17]. These multi-antenna system suffers from inter-element mutual coupling due to in-band fundamental frequency component and there are certain mutual coupling reduction techniques also available in literature to suppress the in-band effect only [18]–[20]. However, in these multi-antenna scenario with high system complexity, the EMI generation due to the HOMs of individual antenna element produces unwanted multi-path scattering between the on-board antennas; this leads to the pattern distortion, beam tilt and generation of unwanted side-lobes [21]–[23].

In this paper, we propose a solution for HOM suppression in compact four-element dual-band MIMO antennas by using a single shorting post near the feed point location, close to antenna center line. We first realize a dual-band microstrip patch element based on CSRR (complementary split-ring resonator) loading concepts [25], [26], and then implement a closely spaced four-element MIMO antenna by sequentially rotating this basic element. The HOM-suppression technique improves the inter-element isolation as well as impedance matching performance of individual antennas in the realized four-element dual-band MIMO antenna. We use full-wave simulation using CST Microwave Studio and experiments on fabricated antenna prototype to validate our proposed HOM suppression technique.

II. DESIGN AND OPERATING MECHANISM OF PROPOSED MIMO ANTENNA

The 3D perspective view of the proposed four-element MIMO antenna is shown in Fig. 1. The antennas are co-axially fed and designed on a Rogers3003 substrate having dimension $L_g \times L_g \times h_1$ (Fig.1) with permittivity and loss-tangent values of $\epsilon_r = 3$, $\tan\delta = 0.001$ respectively. The four antenna elements are loaded with CSRR (Fig. 1) to achieve dual-band operation and size reduction of the overall design. Additionally, four shorting posts realised using plated through hole (PTH) technique are incorporated in four antenna elements to reduce the HOMs and subsequently improve the MIMO antenna mutual coupling and individual antenna impedance matching.

Here, we present the design stages of the proposed MIMO antenna along with its operating mechanism. For each design stage, we examine the surface current distribution, mutual coupling (S_{21}/S_{12}) and impedance matching (S_{11}) levels.

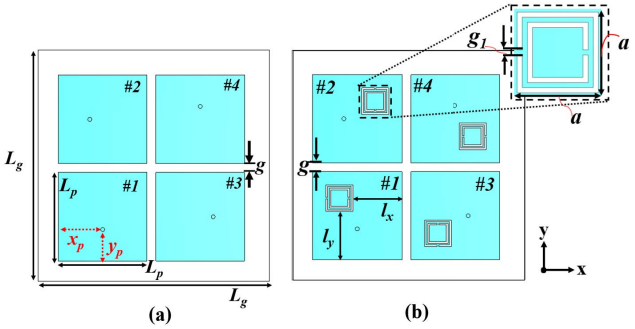

FIGURE 2. Schematic diagrams of: (a) Stage-1, (b) Stage-2 of proposed MIMO antenna design in Fig. 1. Dimensions: $L_g = 52mm$, $L_p = 20mm$, $x_p = 10mm$, $y_p = 6.55mm$, $g = 2\ mm$, $l_x = l_y = 11mm$, $a = 6.01mm$, $g_1 = 0.4mm$.

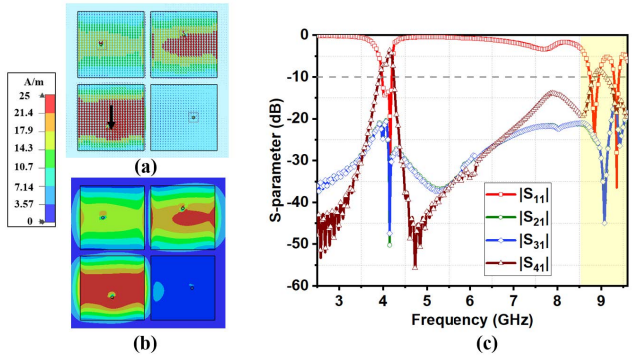

FIGURE 3. (a) Simulated vector surface current distribution on the top-layer patches at 4.1 GHz (b) Simulated scalar Surface current distribution at 4.1 GHz, (Port-1 is excited while terminating all other port to matched load) (c) Frequency variation of S-parameters of design Stage-1 as shown in Fig. 2(a).

A. DESIGN STAGES

- *Stage-1:* Initially, a sequentially rotated probe-fed four-port MIMO system of square microstrip patches (dimensions of $L_p \times L_p$ each) with close inter-element spacing g is designed (Fig. 2(a)). The individual antenna element is designed using microstrip antenna design equations as provided in [27]. The co-axial feed is applied at $x_p = 10mm$ to prevent the orthogonal TM_{01} mode excitation and $y_p = 6.55mm$ to get good impedance matching. The vector surface current distribution corresponding to the radiation mode (see Fig. 3(a))

confirms that the proposed MIMO antenna operates at TM_{10} fundamental patch mode having 4.1 GHz (sub-6 GHz) center frequency with good impedance matching ($|S_{11}| < -10$ dB) (see Fig. 3). The simulated scalar surface current distribution of Fig. 3(b) is plotted to better visualize the fields. Fig. 3(b) shows very strong coupling between the diagonal antenna elements ($|S_{21}| = |S_{12}|$ about -5 dB) due to the same polarisation between the diagonal elements (Fig. 3). Due to the orthogonal antenna arrangement the coupling between the adjacent elements are less compared to the diagonal elements. On the other hand, it is also observed that the MIMO antenna design at stage-1 (Fig. 2(a)) generates the HOMs along with the operating frequency (highlighted part of Fig. 3(c)).

- *Stage-2*: Next, each square patch antenna of Fig. 2(a) is loaded (i.e. etched out from patch surface) with a square CSRR of dimension $a \times a$, located at some offset along the patch diagonal (see Fig. 2(b)). The split-gap and line-width of the ring are kept $0.4mm(g_1)$ (Fig. 2(b)). The CSRR loading generates a second operating frequency at 3.4 GHz and simultaneously shifts the primary operating frequency from 4.1 GHz to 3.9 GHz, leading to the effective electrical area miniaturization of the four-port MIMO antenna by 33.2%.

  Design, Analysis and Placement of CSRR: CSRR (each out from patch) is a high Q-factor resonator, and this can be modelled as LC-shunt resonator tank circuit [28]. The physical dimensions of the CSRR such as square metallic disc backed by ground plane corresponds to the capacitance (C) whereas the square ring perimeter, split gap and the line-width of the ring (g_1) contributes to the inductance (L) of the resonator [28]. To get dual operating mode and to study the effect of CSRR loading in the proposed MIMO antenna the split-gap and the line-width (g_1) is kept at 0.4mm and a parametric study is conducted over CSRR dimension a (see Fig. 4(a)). From Fig. 4(a), it can be inferred that as a is increased there is little variation at 3.9 GHz operating frequency while the second operating frequency is gradually moving towards lower operating region compared to the primary one (i.e., 3.9 GHz). Similarly, the parametric studies are conducted for the position of CSRR on the patch surface as shown in Fig. 4(b) and (c), to get best possible impedance matching and antenna miniaturisation i.e., operating frequency below the unloaded patch antenna (4.1 GHz) with same physical dimensions. From the conducted parametric study the CSRR design parameter, a, and the position (l_x, l_y) are obtained as 6mm and $(11mm, 11mm)$ respectively, which contributes two operating modes such as 3.4 GHz and 3.9 GHz (see the red color plots in Fig. 4). The vector surface current distributions at these operating modes are plotted in Fig. 5 to explain the radiation mechanism. The dominating current direction in the patch at 3.4 GHz and 3.9 GHz are along $\phi = 45^0$ and $\phi = 315^0$ (angles are taken anti-clock wise with respect to x-axis, see bold arrow line in Fig. 5) respectively, which show the CSRR loading produces radiating modes with mutually orthogonal polarisation [26].

  The scalar surface current distribution and S-parameters of the design stage-2 (see Fig. 2(b)) is shown in Fig. 6. The surface current distributions at 3.4 GHz in Fig. 6(a) depicts the existence of coupling between the diagonal elements than the adjacent elements (also confirmed from S-parameter plots in Fig. 6(c)). Moreover, it is also noticed that the existence of spurious HOMs (highlighted part of Fig. 6(c)) in the system. Fig. 7 represents a generalised approximate equivalent circuit model of an isolated patch antenna with CSRR loading of Fig. 2(b). Here, the patch antenna and CSRR along with their corresponding HOMs are represented by series RLC resonators [24], [25]. The coupling in the Fig. 7 describes the interaction (inductive and capacitive) between CSRR fundamental mode to patch fundamental mode and CSRR HOMs to patch HOMs, since CSRR modes radiates along with the patch modes as CSRR its-self is not a good radiator [25]. Here the cross coupling between the fundamental and HOMs of CSRR and patch is neglected. Similarly, when a multi-antenna system placed in a single platform their exist inter-element coupling along with intra-element coupling as shown Fig. 5, which deteriorates the system performance (see Fig. 6(c)). Fig. 8 demonstrates the current distribution at the spurious HOM frequencies (8.3 GHz and 9.4 GHz), showing significant EM interaction between the adjacent antenna elements. Note that, the CSRR-loading leads to dual-band characteristics in the individual patch antennas [25], [26], at 3.4 GHz and 3.9 GHz (see Fig. 6(c)), which was earlier at 4.1 GHz for a unloaded-patch (see Fig. 3(c)). Further, it modifies the HOMs from 8.86 and 9.34 GHz in stage-1 (see Fig. 3(c)) to 7.55 GHz, 8.3 GHz, 8.99 GHz and 9.4 GHz in stage-2. However, only the HOMs at 8.3 and 9.4 GHz have good impedance matched (reflection coefficient less than -10 dB) for the present feeding configuration (see Fig. 6(c)).
- *Stage-3*: The problem of higher-band mutual coupling and EMI due the presence of spurious HOMs encountered in stage-2 is resolved in stage-3 by strategically placing the shorting post very close to the antenna center line, near the feed point location (see Fig. 9). The distance $d_1 = 9.5mm(\approx L_p/2)$ as is decided through parametric studies (see Fig. 9(b)), where it is ensured that best possible impedance matching at the sub-6 GHz frequencies are achieved and unwanted excitation of spurious HOMs are reduced (see Fig. 10(a) for the optimized response). The idea of putting shorting post near the center line, with the goal of disturbing the current distribution of excited spurious HOMs, to implement the

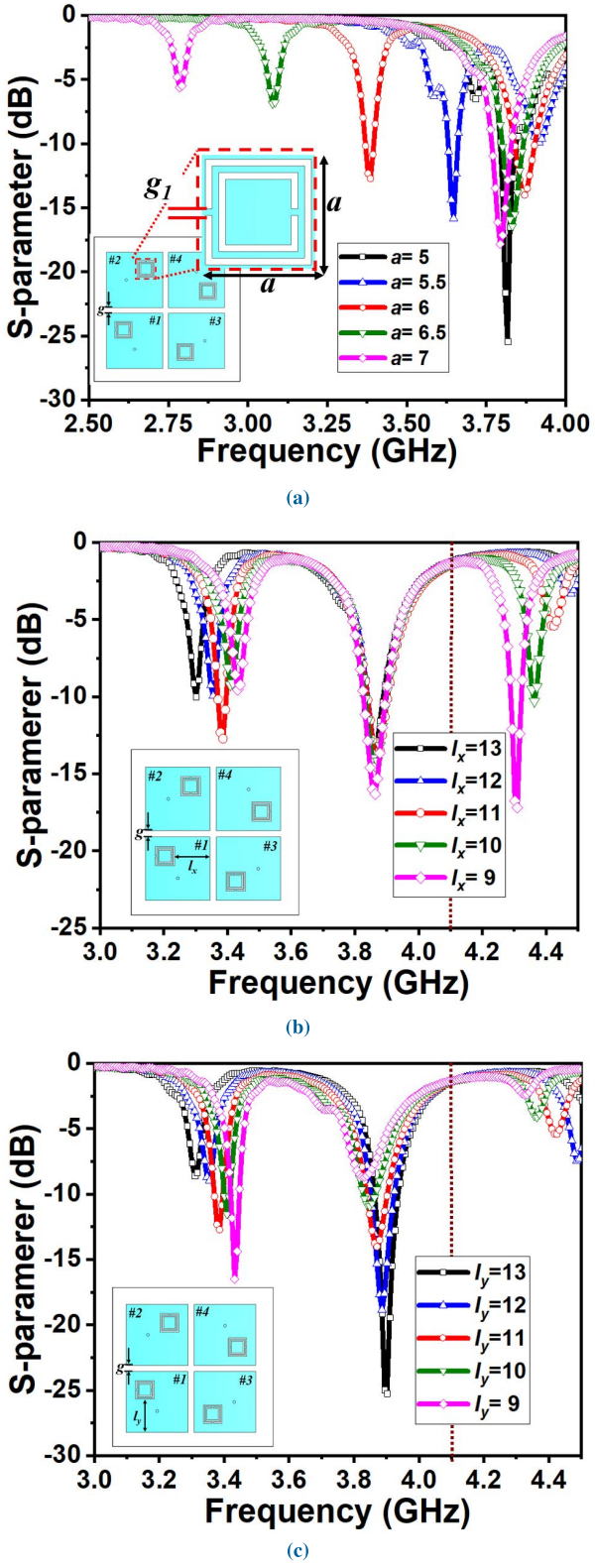

FIGURE 4. Parametric study of: (a) CSRR design parameter a, and CSRR position parameter (b) l_x, (c) l_y to study the impact on S-parameter variation. (Unit: mm).

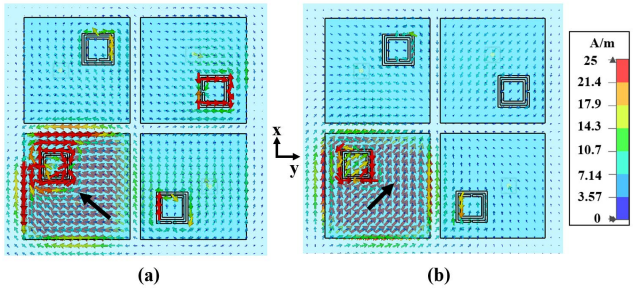

FIGURE 5. Simulated vector surface current distribution on the top-layer patches (port-#1 excited of Fig. 2(b) with other ports terminated in matched load) at: (a) 3.4 GHz and (b) 3.9 GHz.

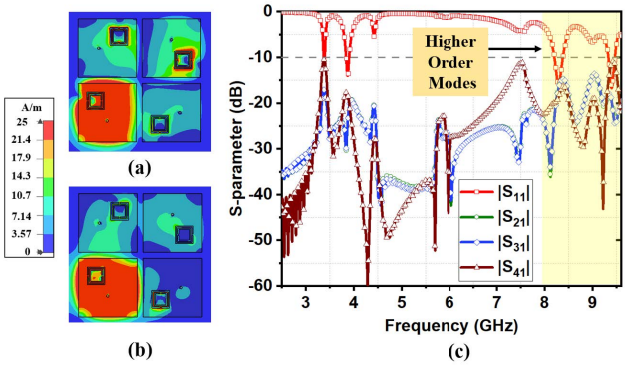

FIGURE 6. Surface current distribution at (a) 3.4 GHz, (b) 3.9 GHz (Port-1 is excited while terminating all other port to matched load), (c) Frequency variation of S-parameters of design Stage-2 of proposed MIMO antenna shown in Fig. 2(b).

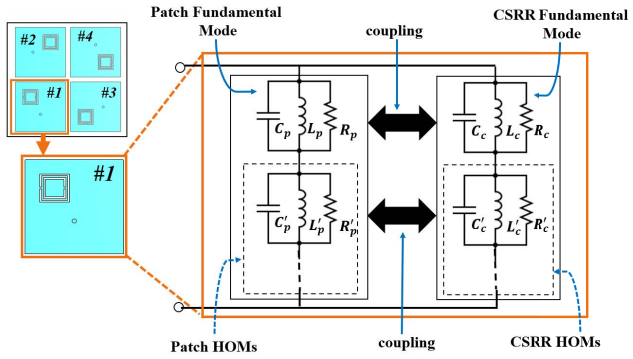

FIGURE 7. Equivalent circuit model of an isolated antenna element of stage-2 (Fig. 2(b)).

maximum current position [27], [29]. Consequently, the surface current distribution at Fig. 10(b) and Fig. 10(c) signifies the reduced coupling compared to Fig. 6(a) and Fig. 6(b), which is also reflected in the S-parameter curves (Fig. 10(a)). Moreover, the placement of shoring post produces 180^0 phase shift in the radiating mode current distributions while keeping the mutually orthogonal mode property intact (see Fig. 11). Fig. 11 depicts the simulated vector surface current distribution showing the dominating current direction (bold arrow mark) along $\phi = 225^0$ and $\phi = 135^0$ (angles are taken anti-clock wise with respect to x-axis) at 3.4 GHz and

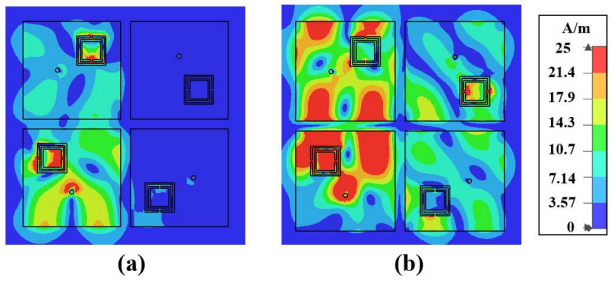

FIGURE 8. Surface current distributions of HOMs at stage-2 as indicated in Fig. 6(c): (a) 8.3 GHz and (b) 9.4 GHz (Port-1 is excited while terminating all other port to matched load).

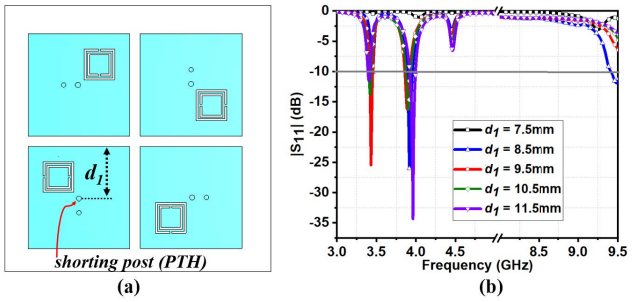

FIGURE 9. Schematic of design: (a) Stage-3, (b) Frequency variation of S-parameters of design Stage-3 for different of PTH position(d_1).

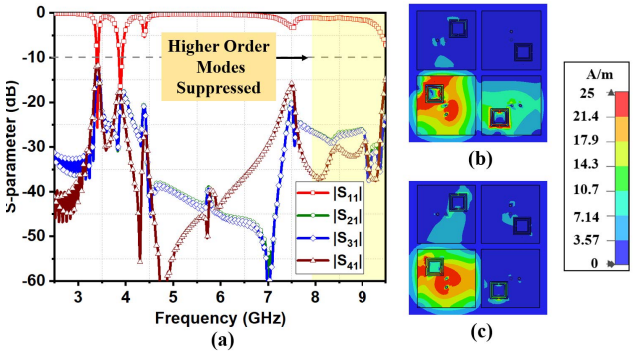

FIGURE 10. (a) Frequency variation of S-parameters of design Stage-3 (Fig. 9(a)), Surface current distribution at (b) 3.4 GHz and (c) 3.9 GHz (Port-1 is excited while terminating all other port to matched load) for the antenna design Stage-3 as shown in Fig. 9(a).

3.9 GHz respectively. Fig. 12(a) and Fig. 12(b) depict the reduced effect of field coupling due to the excitation of HOM compared to Fig. 8(a) and Fig. 8(b) respectively.

The variation of gain over frequency at three design stages are provided in Fig. 13. The antenna gain for stage-1 design (see Fig. 2(a)) is 8.37 dBi at 4.1 GHz. Similarly, the antenna gains for stage-2 (see Fig. 2(b)) and stage-3 (see Fig. 9) are 4.8 dBi / 5.75 dBi and 4.98 dBi / 5.91 dBi respectively at 3.4 GHz / 3.9 GHz. Table 1 shows the comparison of proposed HOMs suppressed design of CSRR-loaded dual-band MIMO antenna with some antenna structures available in

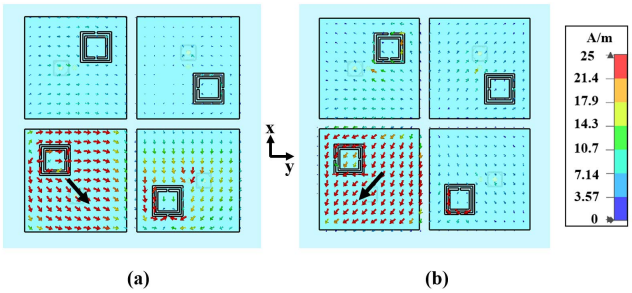

FIGURE 11. Simulated vector surface current distribution on the top-layer patches (port-#1 excited of Fig. 9(a) with other ports terminated in matched load) at: (a) 3.4 GHz and (b) 3.9 GHz.

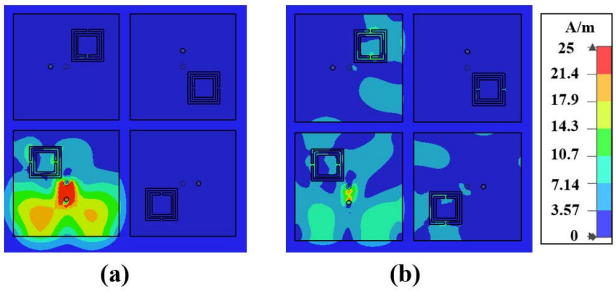

FIGURE 12. Surface current distribution at (a) 8.3 GHz, (b) 9.4 GHz HOMs of design Stage-3 of proposed MIMO antenna shown in Fig. 9(a).

open literature, which depicts the superiority of the proposed work over earlier literature.

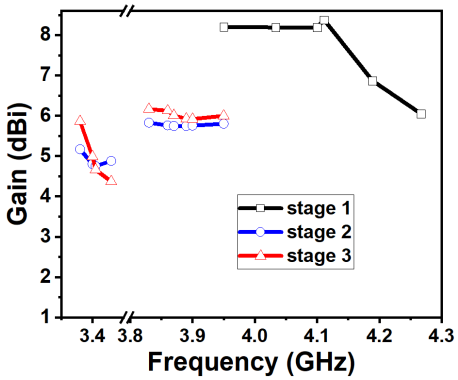

FIGURE 13. Simulated plot for variation of gain over frequency for three stages of antenna design.

III. PROTOTYPE FABRICATION AND MEASUREMENT RESULTS

The fabricated prototype of the proposed four-port CSRR loaded dual band MIMO antenna is shown in Fig. 14. Fig. 14(a) and 14(b) show the top and bottom view of proposed antenna at stage-3 design. The PTH (plated through hole) fabrication process is realised to incorporate the shorting posts. The arrow marks in the Fig. 14(a) show the location of PTHs. The S-parameters for the proposed MIMO antenna are measured using Agilent N5230A PNA and

TABLE 1. Comparison of proposed CSRR-loaded dual-band MIMO antenna with other structures available in open literature.

Ref.	Antenna Type	HOMs suppression technique	Multi-Band Antenna	Gain (dBi)	MIMO configuration
[3]	microstrip patch	photonic band gap	No (0.9 GHz)	-	No
[4]	cavity backed patch	filter	No (3.15 GHz)	> 6.5	No
[7]	microstrip patch	defected ground structure	No (3.1 GHz)	5	No
[8]	microstrip patch	quarter wavelength resonator with capacitive feeding	No (4.9 GHz)	7.8	No
[9]	meander-line annular slot ring antenna	hair pin filter	Yes (2.45/5.8 GHz)	2.2/3.6	No
Prop.	**CSRR loaded patch**	**single shorting post**	**Yes (3.4/3.9 GHz)**	**4.98/5.91**	**Yes**

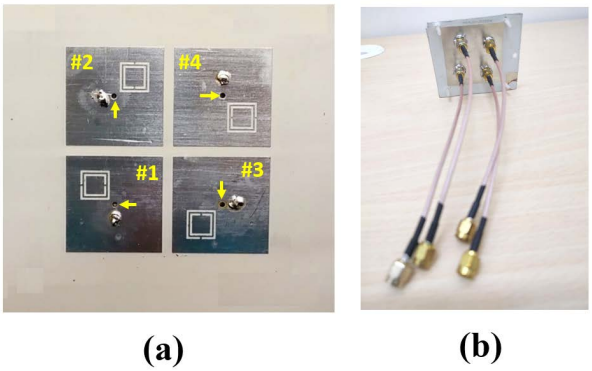

FIGURE 14. Picture of the fabricated MIMO antenna as shown in Fig. 1: (a) top view and (b) bottom views of design stage-3.

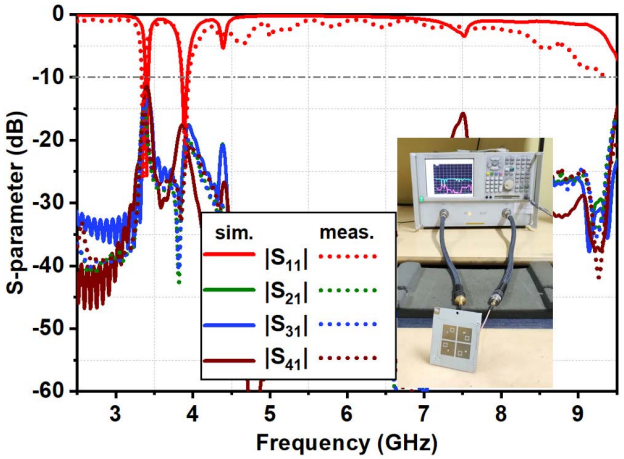

FIGURE 15. Frequency variation of simulated and measured S-parameters of the proposed MIMO antenna (Fig. 1). A picture of measurement set-up is also included.

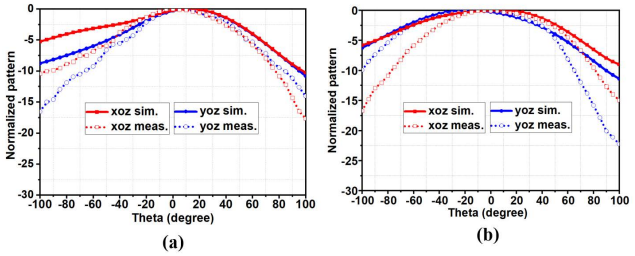

FIGURE 16. Simulated and measured 2D radiation pattern of the proposed MIMO antenna at xoz and yoz plane: (a) 3.4 GHz (b) 3.9 GHz.

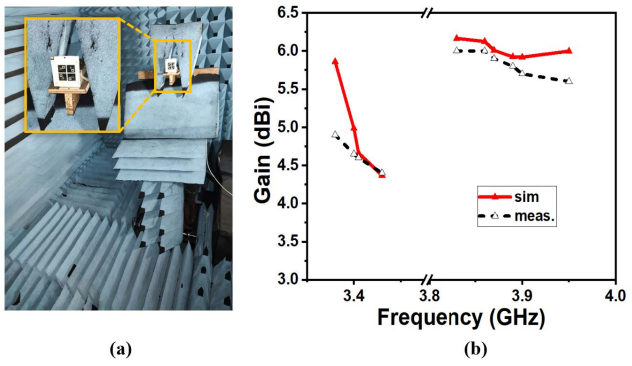

FIGURE 17. (a) Far-field radiation pattern and gain measurement setup inside anechoic chamber, (b) Simulated and measured variation of gain over frequency of the proposed MIMO antenna.

provided in Fig. 15. The simulated and measured 2D radiation patterns of the final antenna (stage-3) design at 3.4 GHz and 3.9 GHz operating frequencies are provided in Fig. 16 (a) and (b) respectively. The radiation patterns at xoz and yoz 2D planes in Fig. 16 indicate that the antenna radiates in broad side direction at its operating frequencies. The far-field radiation pattern measurement set-up inside anechoic chamber is shown in Fig. 17 (a). Fig. 17 (b) depicts the simulated and measured gain plot over frequency of the final antenna (stage-3) stage. The measured gain at 3.4 GHz and 3.9 GHz operating frequencies are 4.6 dBi and 5.7 dBi respectively. The measured S-parameters, radiation patterns and the gain plot are in good agreement with the simulated ones.

A. MIMO PERFORMANCE PARAMETERS

MIMO performance of the proposed four-port antenna configuration of Fig. 1 is assessed by computation of total active reflection coefficient (*TARC*), envelop correlation coefficient (*ECC*) and channel capacity loss (*CCL*) in the operating bands. *TARC* considers the constructive or destructive signal combination from one port to another port while evaluating MIMO antenna reflection co-efficient i.e. it indicates MIMO antenna working capability when all ports are excited simultaneously [30]. Similarly, *ECC* measures the coupling in the field patterns between the antenna elements in a MIMO system, which described the diversity performance of a MIMO antenna system [31]. *CCL* indicates the upper bound of reliable signal transmission by the MIMO antenna system [32]. For details on *TARC, ECC, CCL* please refer to [30]–[32]. Fig. 18 shows that the proposed MIMO configuration exhibits the polarisation and pattern diversity by

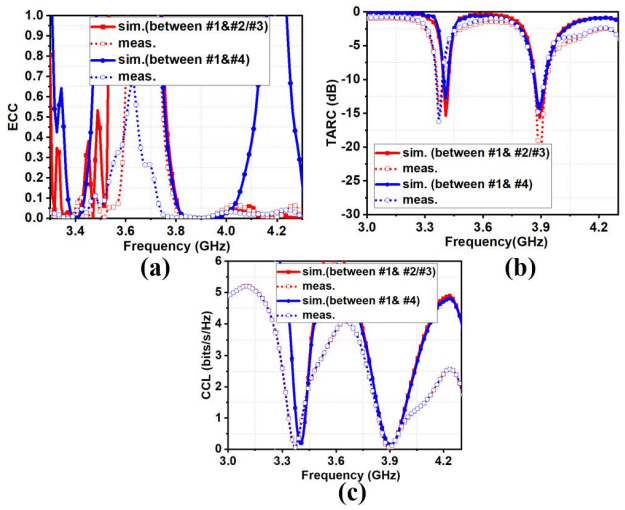

FIGURE 18. Frequency variation of proposed four port MIMO antenna performance metrics: (a) *TARC*, (b) *ECC*, and (c) *CCL*.

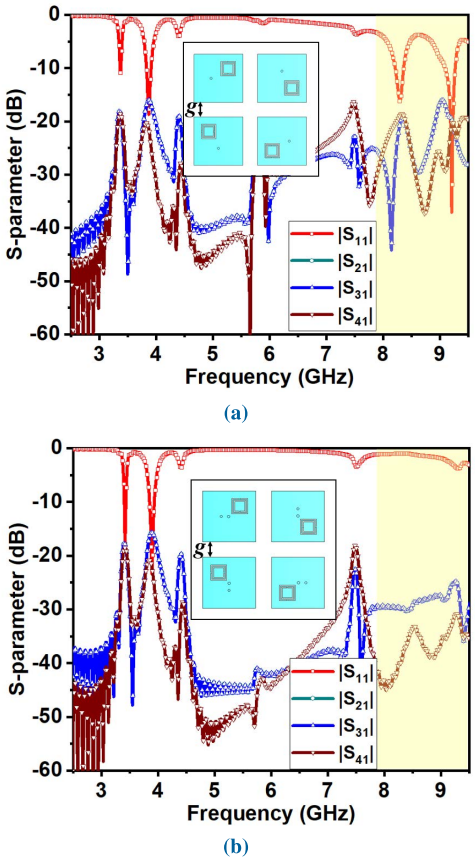

FIGURE 19. Simulated frequency variation of S-parameter for the proposed MIMO antenna design having 6 mm inter-element spacing (*g*) (a) without shorting post showing poor impedance matching and presence of HOMs, (b) with shorting post showing good impedance matching, reduced mutual coupling (<−15 dB) and suppressed HOMs.

virtue of its sequentially rotated arrangement [18]. The value of *ECC* is much less than 0.5 for uniform propagation environment, indicating the excellent diversity performance; this is further reflected in the low value of channel capacity loss (<0.5 bits/s/Hz) in the operating bands. Also, the *TARC* being less than −10 dB at operating bands indicates that the four-port system is capable of operating efficiently in "active" (simultaneous port-excitation) condition.

- *Note:* The aforementioned MIMO performance analysis shows the satisfactory results for the present form of the proposed design which are evaluated based on the S-parameter data shown in Fig. 15 i.e., $|S_{11}| < -10$ dB at 3.4 GHz and 3.9 GHz; similarly, $|S_{21}| = |S_{31}| = |S_{41}| < -11$ dB at 3.4 GHz and <−15 dB at 3.9 GHz. However, the mutual coupling between the antenna elements can further be improved based on application scenarios like massive MIMO base station antenna design needs mutual coupling below <−20 dB and most 5G hand-held antenna system need mutual coupling <−15 dB (for more information refer [33]–[40]). Therefore, to get the intended result we can slightly increase the antenna spacing in the proposed MIMO configuration. An extended design of the proposed work by increasing the inter-element spacing ($g = 6$ mm) is provided in Fig. 19. Fig. 19(a) shows MIMO configuration without shorting post exhibits poor impedance matching and the presence of HOMs (highlighted part). MIMO configuration with shorting post is shown in Fig. 19(b) which exhibits good impedance matching and mutual coupling <−15 dB at 3.4 GHz and 3.9 GHz both. It can also be noticed that the HOMs are also suppressed (highlighted part in Fig. 19(b)), which signifies that the proposed HOM reduction technique is independent of variation of inter-element spacing.

IV. CONCLUSION

In this work, the design steps of a four-port CSRR loaded dual band MIMO antenna are provided. Then, we proposed a very simple solution to suppress the HOMs in the MIMO antenna by inserting a single shorting post near the feed-location of each CSRR-loaded patch, which eventually improves both impedance matching (<−15 dB) and mutual coupling (<−11 dB) levels. S-parameters and 2D radiation patterns of the fabricated antenna prototype are measured and compared with simulation results from CST MWS. Note that, due to the inherent nature of the microstrip antenna, the proposed MIMO configuration exhibits narrow impedance bandwidth of 40 MHz and 70 MHz respectively at 3.4 GHz and 3.9 GHz bands. However, these achieved bandwidth levels are sufficient for the application in sub-6 GHz n77 band [41]. Furthermore, the calculated MIMO parameters indicate good diversity performance of the proposed four-element configuration. The proposed four-element sub-array design could be suitable for 5G massive-MIMO application, where the proposed suppressed spurious HOMs would be helpful to prevent interoperability problem in 5G system [42] (i.e., out-of-band interference of sub-6 GHz band on 5G mm-wave bands, which reduced receiver sensitivity).

ACKNOWLEDGMENT

The authors would like to thank Prof. K. J. Vinoy, the Chair, Department of ECE, IISc, Bengaluru, for providing the measurement facilities (PNA and Anechoic Chamber).

REFERENCES

[1] C. A. Balanis, *Antenna Theory: Analysis and Design*. Hoboken, NJ, USA: Wiley, 2016.
[2] K. C. Gupta and P. S. Hall, *Analysis and Design of Integrated Circuit Antenna Modules*. New York, NY, USA: Wiley, 2000.
[3] Y. Horii and M. Tsutsumi, "Harmonic control by photonic bandgap on microstrip patch antenna," *IEEE Microw. Guided Wave Lett.*, vol. 9, no. 1, pp. 13–15, Jan. 1999.
[4] J. Yun, S. Trinh-Van, J.-Y. Park, Y. Yang, K.-Y. Lee, and K. C. Hwang, "Cavity-backed patch filtenna for harmonic suppression," *IEEE Access*, vol. 8, pp. 221580–221589, 2020.
[5] A. J. Alazemi and G. M. Rebeiz, "A tunable single-feed triple-band LTE antenna with harmonic suppression," *IEEE Access*, vol. 7, pp. 104667–104672, 2019.
[6] S. Kwon, B. M. Lee, Y. J. Yoon, W. Y. Song, and J.-G. Yook, "A harmonic suppression antenna for an active integrated antenna," *IEEE Microw. Wireless Compon. Lett.*, vol. 13, no. 2, pp. 54–56, Feb. 2003.
[7] S. Biswas, D. Guha, and C. Kumar, "Control of higher harmonics and their radiations in microstrip antennas using compact defected ground structures," *IEEE Trans. Antennas Propag.*, vol. 61, no. 6, pp. 3349–3353, Jun. 2013.
[8] J.-D. Zhang, L. Zhu, Q.-S. Wu, N.-W. Liu, and W. Wu, "A compact microstrip-fed patch antenna with enhanced bandwidth and harmonic suppression," *IEEE Trans. Antennas Propag.*, vol. 64, no. 12, pp. 5030–5037, Dec. 2016.
[9] Y. J. Ren, M. F. Farooqui, and K. Chang, "A compact dual-frequency rectifying antenna with high-orders harmonic-rejection," *IEEE Trans. Antennas Propag.*, vol. 55, no. 7, pp. 2110–2113, Jul. 2007.
[10] C. X. Mao, S. Gao, Y. Wang, and Z. Cheng, "Filtering antenna with two-octave harmonic suppression," *IEEE Antennas Wireless Propag. Lett.*, vol. 16, pp. 1361–1364, 2017.
[11] G. R. Nikandish, R. B. Staszewski, and A. Zhu, "A fully integrated GaN dual-channel power amplifier with crosstalk suppression for 5G massive MIMO transmitters," *IEEE Trans. Circuits Syst. II, Exp. Briefs*, vol. 68, no. 1, pp. 246–250, Jan. 2021.
[12] C. Li, M. Li, M. Verhelst, A. Bourdoux, L. Van der Perre, and S. Pollin, "On the general mathematical framework, calibration/compensation method, and applications of non-ideal software defined harmonics rejection transceivers," in *IEEE Trans. Circuits Syst. I, Reg. Papers*, vol. 62, no. 1, pp. 292–301, Jan. 2015.
[13] T. L. Marzetta, E. G. Larsson, H. Yang, and H. Q. Ngo, *Fundamentals Massive MIMO*. Cambridge, U.K.: Cambridge Univ. Press, 2016.
[14] E. Björnson, J. Hoydis, and L. Sanguinetti, "Massive MIMO networks: Spectral, energy, and hardware efficiency," *Found. Trends Signal Process.*, vol. 11, nos. 3–4, pp. 154–655, 2017.
[15] O. Saatlou, M. O. Ahmad, and M. N. S. Swamy, "Spectral efficiency maximization of multiuser massive MIMO systems with finite-dimensional channel via control of users' power," *IEEE Trans. Circuits Syst. II, Exp. Briefs*, vol. 65, no. 7, pp. 883–887, Jul. 2018.
[16] M. Mahdavi, O. Edfors, V. Owall, and L. Liu, "A low latency and area efficient FFT processor for massive MIMO systems," in *Proc. IEEE Int. Symp. Circuits Syst. (ISCAS)*, May 2017, pp. 1–4.
[17] D. Sarkar, S. M. Mikki, and Y. M. M. Antar, "Eigenspace structure estimation for dual-polarized massive MIMO systems using an IDM-CGF technique," *IEEE Antennas Wireless Propag. Lett.*, vol. 18, no. 4, pp. 781–785, Apr. 2019.
[18] N. Kalva, J. C. Dash, and J. Mukherjee, "Closely spaced dual-band quad-element compact MIMO antenna with polarization and pattern diversity," in *Proc. IEEE Int. Symp. Antennas Propag. North Amer. Radio Sci. Meeting*, Jul. 2020, pp. 1567–1568.
[19] I. Nadeem and D.-Y. Choi, "Study on mutual coupling reduction technique for MIMO antennas," *IEEE Access*, vol. 7, pp. 563–586, 2019.
[20] H. A. Mashagba, H. A. Rahim, I. Adam, M. H. Jamaluddin, M. N. M. Yasin, M. Jusoh, T. Sabapathy, M. Abdulmalek, A. A. Al-Hadi, A. M. Ismail, and P. J. Soh, "A hybrid mutual coupling reduction technique in a dual-band MIMO textile antenna for WBAN and 5G applications," *IEEE Access*, vol. 9, pp. 150768–150780, 2021.
[21] R. F. Harrington, "Theory of loaded scatterers," *Proc. Inst. Elect. Eng.*, vol. 111, no. 4, pp. 617–623, Apr. 1964.
[22] A. C. Gately, D. J. R. Stock, and B. R. S. Cheo, "A network description for antenna problems," *Proc. IEEE*, vol. 56, no. 7, pp. 1181–1193, Jul. 1968.
[23] F. H. Lin and Z. N. Chen, "A method of suppressing higher order modes for improving radiation performance of metasurface multiport antennas using characteristic mode analysis," *IEEE Trans. Antennas Propag.*, vol. 66, no. 4, pp. 1894–1902, Apr. 2018.
[24] Z.-X. Liu, L. Zhu, and N.-W. Liu, "A compact omnidirectional patch antenna with ultrawideband harmonic suppression," *IEEE Trans. Antennas Propag.*, vol. 68, no. 11, pp. 7640–7645, Nov. 2020.
[25] Y. Dong, H. Toyao, and T. Itoh, "Design and characterization of miniaturized patch antennas loaded with complementary split-ring resonators," *IEEE Trans. Antennas Propag.*, vol. 60, no. 2, pp. 772–785, Feb. 2012.
[26] D. Sarkar, Y. Antar, and S. Mikki, "Four-port CSRR-loaded dual-band dual-mode patch sub-array for massive MIMO applications," in *Proc. IEEE Int. Symp. Antennas Propag. North Amer. Radio Sci. Meeting*, Jul. 2020, pp. 1731–1732.
[27] G. Kumar and K. P. Ray, *Broadband Microstrip Antennas*. Norwood, MA, USA: Artech House, 1996.
[28] J. D. Baena, J. Bonache, F. Martín, R. M. Sillero, F. Falcone, T. Lopetegi, M. A. G. Laso, J. Garcia-Garcia, I. Gil, M. F. Portillo, and M. Sorolla, "Equivalent-circuit models for split-ring resonators and complementary split-ring resonators coupled to planar transmission lines," *IEEE Trans. Microw. Theory Techn.*, vol. 53, no. 4, pp. 1451–1461, Apr. 2005.
[29] R. Garg, P. Bhartia, I. Bahl, and A. Ittipiboon, *Microstrip Antenna Design Handbook*. Norwood, MA, USA: Artech House, 2001.
[30] M. S. Sharawi, "Printed MIMO antenna systems: Performance metrics implementations and challenges," *Proc. Forum Electromagn. Res. Methods Appl. Technol. (FERMAT)*, vol. 1, 2014, pp. 1–11.
[31] Y. Sharma, D. Sarkar, K. Saurav, and K. Srivastava, "Three-element MIMO antenna system with pattern and polarization diversity for WLAN applications," *IEEE Antennas Wireless Propag. Lett.*, vol. 16, pp. 1163–1166, 2017.
[32] S. Dey, S. Dey, and S. K. Koul, "Isolation improvement of MIMO antenna using novel EBG and hair-pin shaped DGS at 5G millimeter wave band," *IEEE Access*, vol. 9, pp. 162820–162834, 2021.
[33] Z. Ji, Y. Guo, Y. He, L. Zhao, G.-L. Huang, C. Zhou, Q. Zhang, and W. Lin, "Low mutual coupling design for 5G MIMO antennas using multi-feed technology and its application on metal-rimmed mobile phones," *IEEE Access*, vol. 9, pp. 151023–151036, 2021.
[34] Y. Zhu, Y. Chen, and S. Yang, "Cross-band mutual coupling reduction in dual-band base-station antennas with a novel grid frequency selective surface," *IEEE Trans. Antennas Propag.*, vol. 69, no. 12, pp. 8991–8996, Dec. 2021.
[35] Y. Da, Z. Zhang, X. Chen, and A. A. Kishk, "Mutual coupling reduction with dielectric superstrate for base station arrays," *IEEE Antennas Wireless Propag. Lett.*, vol. 20, no. 5, pp. 843–847, May 2021.
[36] Y. Liu, X. Yang, Y. Jia, and Y. J. Guo, "A low correlation and mutual coupling MIMO antenna," *IEEE Access*, vol. 7, pp. 127384–127392, 2019.
[37] H. R. D. Filgueiras and A. C. S. Junior, "A 64-element and dual-polarized SICL-based slot antenna array development applied to TDD massive MIMO," *IEEE Antennas Wireless Propag. Lett.*, early access, Jan. 25, 2022, doi: 10.1109/LAWP.2022.3144916.
[38] A. Iqbal, O. A. Saraereh, A. W. Ahmad, and S. Bashir, "Mutual coupling reduction using F-shaped stubs in UWB-MIMO antenna," *IEEE Access*, vol. 6, pp. 2755–2759, 2018.
[39] J.-D. Park, M. Rahman, and H. N. Chen, "Isolation enhancement of wideband MIMO array antennas utilizing resistive loading," *IEEE Access*, vol. 7, pp. 81020–81026, 2019.
[40] A. A. Megahed, M. Abdelazim, E. H. Abdelhay, and H. Y. M. Soliman, "Sub-6 GHz highly isolated wideband MIMO antenna arrays," *IEEE Access*, vol. 10, pp. 19875–19889, 2022.

[41] *Technical Specification: 5G; NR; User Equipment (UE) Radio Transmission and Reception;Part 1: Range 1 Standalone*, document TS 38.101-1 Version 15.2.0 Release 15, 3GPP. [Online]. Available: https://www.etsi.org/delive/etsits/138100138199/13810101/15.02.0060/ts13810101v150200p.pdf
[42] M. E. Leinonen, N. Tervo, O. Kursu, and A. Parssinen, "Out-of-band interference in 5G mmW multi-antenna transceivers: Co-existence scenarios," in *Proc. Eur. Conf. Netw. Commun. (EuCNC)*, Jun. 2018, pp. 1–9.

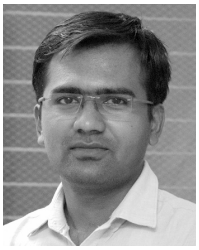

JOGESH CHANDRA DASH (Member, IEEE) received the M.Tech. degree in electronics and tele-communication engineering with RF and microwave specialization from VSSUT (formerly UCE), Burla, in 2016, and the Ph.D. degree in electrical engineering with specialization in communication and signal processing: (RF and microwave) (EE1) from the Indian Institute of Technology (IIT), Mumbai, in 2021. He is currently working as a Postdoctoral Research Associate with the iDARE Laboratory, Department of Electrical Communication Engineering, Indian Institute of Science (IISc), Bengaluru. He serves as a reviewer in several journals, such as IEEE TRANSACTIONS ON INDUSTRIAL ELECTRONICS, IEEE ACCESS, *IET Microwave, Antenna, & Propagation*, and *International Journal of RF and Computer-Aided Engineering* (Wiley).

DEBDEEP SARKAR (Member, IEEE) received the B.E. degree in ETCE from Jadavpur University, in 2011, and the M.Tech. and Ph.D. degrees from the Indian Institute of Technology, Kanpur, in 2013 and 2018, respectively.

He has worked as a Visiting Researcher and a Postdoctoral Fellow with the Royal Military College, Canada, from May 2017 to August 2017 and from November 2018 to February 2020, respectively. He is currently an Assistant Professor with the Department of Electrical Communication Engineering (ECE), Indian Institute of Science (IISc), Bengaluru. He has authored/coauthored more than 30 peer-reviewed journal articles. He serves as a reviewer in several prestigious journals, such as IEEE TRANSACTIONS ON ANTENNAS AND PROPAGATION, IEEE TRANSACTIONS ON MICROWAVE THEORY AND TECHNIQUES, IEEE TRANSACTIONS ON VEHICULAR TECHNOLOGY, IEEE ANTENNAS AND WIRELESS PROPAGATION LETTERS, and *IEEE Antennas and Propagation Magazine*.

Dr. Sarkar was a recipient of the URSI Young Scientist Award (YSA) twice (in the APRASC 2019 and URSIGASS 2020), along with best paper awards and grants from several conferences. He has been selected for the prestigious position of "Infosys Young Investigator," by Infosys Foundation, Bengaluru. He is currently an IEEE Antennas and Propagation Society Young Professionals (YP) Committee Member and the Vice-Chair in the IEEE YP Affinity Group, Bengaluru Section. He is also serving as an Associate Editor for IEEE ACCESS and *IET Microwaves, Antennas & Propagation*.